AIMS Mathematics, 10(11): 26418–26445.
DOI: 10.3934/math.20251161
Received: 02 August 2025
Revised: 29 October 2025
Accepted: 05 November 2025
Published: 17 November 2025

https://www.aimspress.com/journal/Math

Research article

Starvation-recovery dynamics: insights via a nutritional state-structured model

Saiful Rahman Mondal*

Department of Mathematics and Statistics, College of Science, King Faisal University, P.O. Box 400, Al-Ahsa 31982, Saudi Arabia

* **Correspondence:** Email: smondal@kfu.edu.sa.

Abstract: This paper presents a nutritional state-structured model (NSM) to explore the dynamics of starvation and recovery in consumer-resource systems, focusing on full consumers (F), hungry consumers (H), and resources (R). The model employs a system of differential equations to capture ecological processes such as reproduction, starvation, and resource regeneration. Through bifurcation analysis, we identified critical thresholds, notably the starvation rate (σ) relative to the reproduction rate (λ), that dictate system stability, transitioning between extinction and coexistence equilibria. Parameter sensitive and numerical simulations revealed how parameter variations influence population persistence and resource sustainability, with $\sigma > \lambda$ promoting balanced ecosystems and $\lambda > \sigma$ leading to potential overexploitation. The analogue of the basic reproduction number ($\mathcal{R}_e$) was derived using the next-generation matrix method, providing insights into the invasion dynamics and stability conditions of the system. This framework serves as a robust tool for analyzing eco-evolutionary interactions and assessing population persistence under resource-limited conditions. Finally, we demonstrated how higher fat reserves enhance competitive advantage, thereby driving the evolutionary trend toward larger body sizes as predicted by Cope's rule.

Keywords: starvation dynamics; resource replenishment; differential equations; ecological modeling
Mathematics Subject Classification: 34B15, 34C60, 34D23, 35C07

1. Introduction

Organisms constantly face the challenge of allocating limited energy resources to competing physiological demands, particularly between somatic maintenance and reproductive effort. This fundamental tradeoff lies at the heart of behavioral ecology and is shaped by both internal energetic states and external environmental uncertainties [13, 14, 29]. The timing and magnitude of energy investment in reproduction are subject to natural selection, as these decisions have direct implications

for survival and future fitness outcomes [12, 22].

Resource availability, or the lack thereof, exerts a profound influence on an organism's ability to sustain essential functions and initiate reproduction. Nutritional constraints can lead to adaptive shifts in life-history strategies, including delayed or suppressed reproductive events. Such effects are observable across a wide range of taxa—from irregular menstrual cycling and increased rates of spontaneous abortion in mammals under nutritional stress [1, 11] to the direct regulation of growth and division in unicellular organisms based on resource abundance [29]. Understanding the dynamics of consumer-resource interactions is pivotal in ecological modeling. Resource availability and consumer behavior are deeply intertwined, particularly under the constraints imposed by starvation, which can influence foraging strategies, reproductive timing, and survival rates. Mathematical modeling has been widely used to understand the transmission dynamics of infectious diseases. For instance, in [31], the authors have modeled the interaction between the complement system (CS) and bacterial infections using nonlinear ODE frameworks. These models, incorporating functional responses like the Hill hazard function, show that the CS can eliminate, suppress, or be overwhelmed by bacterial invaders depending on system strength. Bifurcation analysis further highlights how changes in parameters affect infection outcomes, emphasizing the role of both innate and adaptive immunity in disease progression.

Similarly, compartmental models such as the SEIR (Susceptible Exposed Infectious Recovered)–SEI (Susceptible Exposed Infectious) framework have been employed to describe the transmission dynamics of vector-borne diseases like dengue. In these models, determining the key parameters influencing disease transmission is critical. Sensitivity analysis serves as an essential tool in identifying which parameters most significantly impact the spread of infection. For example, Chitnis et al. performed a sensitivity analysis to determine important parameters in the spread of malaria [5]. Further studies by Shah and Gupta, and Rodrigues et al., also used sensitivity analysis to assess the relative importance of model parameters in understanding disease transmission dynamics [25].

Mathematical modeling has been widely used to understand the transmission dynamics of infectious diseases. For instance, Diekmann et al. introduced the concept and methods for computing the basic reproduction ratio $\mathcal{R}_0$ in structured populations [8], which was further extended by Van den Driessche and Watmough to explore reproduction numbers and sub-threshold endemic equilibria in compartmental models [28]. Recently, in [4], the studies present deterministic SIR-type models to analyze the spread of the Zika virus in Brazil, using published epidemic data. Parameter estimation is achieved through a hybrid optimization method combining stochastic search and heuristic descent, improving computational efficiency. The models are validated against real data, and the estimated basic reproduction number aligns with values reported in the literature. Several studies have used compartmental models to estimate transmission dynamics and reproduction numbers during infectious disease outbreaks. Adaptive SIR models have been applied to COVID-19 data for real-time tracking [26], while multi-wave dynamics have been captured using effective reproduction number modeling [23]. Foundational methods for estimating the reproduction number from outbreak data were developed in [7]. Recent advancements in bifurcation theory have offered powerful tools for analyzing complex dynamical behaviors across a range of applied systems. For instance, Elsadany et al. [10] examined bifurcation structures in discrete ecological models, whereas Margenov et al. [19], in the context of epidemiological modeling, applied these techniques to an SEIRS model that incorporates vaccination and hospitalization dynamics. Magnitskii [18] demonstrated that transitions to chaos in chemical and biological systems follow the universal Feigenbaum–Sharkovsky–Magnitskii

(FShM) bifurcation theory through subharmonic and homoclinic cascades of limit cycles. In [2, 3], mathematical models incorporating age structure and time delays were developed to analyze complex dynamics in epidemiological and social contexts—specifically, a double age-dependent SIRS model with incubation and immunity delays, and an age-structured heroin transmission model with a remission delay. Both studies focus on the emergence of Hopf bifurcation and support their theoretical findings with numerical simulations, highlighting implications for disease control and public health. Several recent studies have employed mathematical modeling and bifurcation analysis to investigate complex biological systems. In [16], a fractional-order immune response model for conjunctivitis was developed using the ABC operator, with stability, bifurcation, and sensitivity analyses confirming the model's robustness under early detection and treatment scenarios. In [21] analyzed soliton dynamics in a (3 + 1)-dimensional p-type model using bifurcation and chaos theory, while [15] explored fixed points and bifurcation behavior in a discrete predator–prey system. Similarly, [24] examined a discrete-time plant–herbivore model, identifying Neimark–Sacker and transcritical bifurcations and applying chaos control techniques. In addition, [20] investigated predator–prey interactions with harvesting and social behavior, revealing Hopf and Turing-Hopf bifurcations through reaction-diffusion analysis. Together, these studies underscore the broad applicability of bifurcation theory in analyzing complex dynamics across physical and biological systems. Similarly, mathematical models in ecology have long been employed to capture interactions between species and their environments. Beyond epidemiological applications, the Lotka–Volterra equations have played a foundational role in mathematical biology, describing interactions between predator and prey populations through coupled nonlinear dynamics [17,32]. These classical models capture how interspecific interactions and resource limitation drive oscillatory population behavior and have inspired a vast body of theoretical work exploring ecological stability, coexistence, and bifurcation phenomena [6, 9, 27]. Our nutritional state-structured model (NSM) is conceptually related to this tradition in that it also represents population interactions through coupled differential equations. However, rather than modeling predator–prey encounters, the NSM focuses on transitions between nutritional states—*full* and *hungry* consumers—linking individual energetic balance to population persistence.

In this work, we study the nutrition-structured model introduced in [30], which builds upon the framework of the starving random walk paradigm. The model emphasizes transitions between two key nutritional states: *full* and *hungry*. Consumers in the full state become hungry as local resources are depleted, while hungry individuals can recover to the full state upon encountering and consuming resources. The system comprises three state variables: full consumers (F), hungry consumers (H), and resources (R). Their dynamics are governed by the following equations:

$$\dot{F} = \lambda F + \xi\rho RH - \sigma(1 - R)F, \tag{1.1a}$$

$$\dot{H} = \sigma(1 - R)F - \xi\rho RH - \mu H, \tag{1.1b}$$

$$\dot{R} = \alpha(1 - R)R - (\rho R + \delta)H - \beta F. \tag{1.1c}$$

The mathematical model consists of three state variables: full consumers (F), hungry consumers (H), and resources (R), whose dynamics are described by a system of differential equations. The first equation captures the changes in the full consumer population. Full consumers reproduce at a rate proportional to their population, denoted by λF, recover from the hungry state at a rate $\xi\rho RH$, and the term $\sigma(1 - R)F$ denotes the rate at which full consumers become hungry due to limited resources. When resources are abundant ($R \to 1$), starvation is negligible, whereas when resources are scarce

($R \to 0$), all full consumers experience starvation at the maximum rate σF. Thus, $(1 - R)$ smoothly scales starvation pressure with resource scarcity. The second equation describes the dynamics of hungry consumers. These individuals are replenished by transitions from the full state at the same starvation rate, $\sigma(1 - R)F$, recover back to the full state at a rate $-\xi\rho RH$, and experience mortality at a rate μH.

The third equation governs the dynamics of the resource population. Resources grow logistically at a rate $\alpha(1 - R)R$, reflecting a density-dependent replenishment process. They are consumed by hungry consumers at a rate proportional to their abundance, ρRH, and by full consumers at a constant rate, βF. Additionally, hungry consumers require a baseline resource for maintenance, depleting resources at a fixed rate δ. Together, these equations encapsulate the interplay between consumer states and resource availability, providing a comprehensive framework for understanding the eco-evolutionary dynamics of starvation and recovery. Parameters are constrained by allometric scaling with body mass M, e.g., $\lambda \propto M^{-3/4}$, $\sigma \propto M^{-1/4}$, $\rho \propto M^{-1/4}$, reflecting metabolic rates. Body fat percentage is parameterized by χ, where $\chi > 0$ indicates higher fat reserves, reducing σ and increasing ρ.

This Figure 1 illustrates the starvation-recovery model, showing the interactions among full consumers (F), hungry consumers (H), and resources (R). Full consumers reproduce at rate λF and transition to hungry consumers due to starvation at rate $\sigma(1 - R)F$. Hungry consumers can recover to the full state at rate $\xi\rho RH$ or die at rate μH. Resources grow logistically at a rate $\alpha(1 - R)R$ and are consumed by both hungry consumers at a rate $(\rho R + \delta)H$ and full consumers at a rate βF.

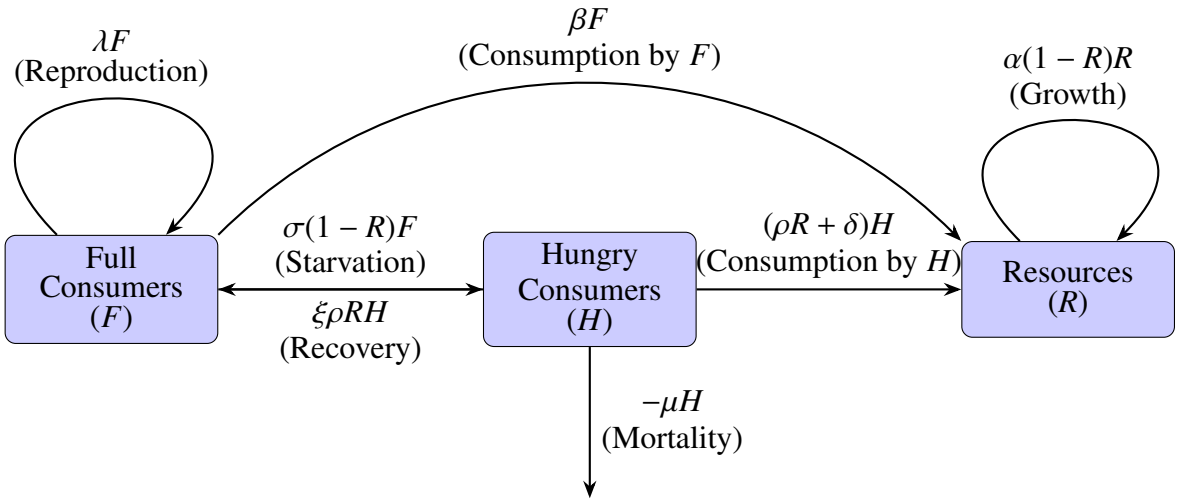

Figure 1. Starvation–recovery model showing interactions among full consumers (F), hungry consumers (H), and resources (R).

Let the total population be defined as the sum of full consumers and hungry consumers,

$$N(t) = F(t) + H(t).$$

To find the dynamics of the total population, we differentiate with respect to time:

$$\dot{N} = \dot{F} + \dot{H}.$$

Substituting from the system of equations:

$$\dot{F} = \lambda F + \xi\rho RH - \sigma(1-R)F,$$
$$\dot{H} = \sigma(1-R)F - \xi\rho RH - \mu H,$$

and we get

$$\begin{aligned}\dot{N} &= (\lambda F + \xi\rho RH - \sigma(1-R)F) + (\sigma(1-R)F - \xi\rho RH - \mu H)\\ &= \lambda F - \mu H.\end{aligned}$$

Therefore, the total population changes according to

$$\dot{N} = \lambda F - \mu H.$$

The reproduction rate is independent of resource density because full consumers allocate a fixed amount of energy toward reproduction, regardless of how much resource is available. In contrast, hungry consumers allocate no energy to reproduction. Similarly, the maintenance costs for consumers in both the full (F) and hungry (H) states are also unaffected by resource levels, as they represent the baseline energetic requirements necessary for survival in each state.

The paper is organized as follows: Section 2 introduces the model parameters and provides their biological interpretation, emphasizing connections to metabolic scaling. Section 3 presents a stability analysis of the system's equilibrium points to determine conditions for local stability. Section 4 examines the dissipative nature of the system and establishes criteria for the persistence of consumer and resource populations. In Section 5, we derive the ecological analogue of the basic reproduction number, denoted by $\mathcal{R}_e$, and discuss its implications for consumer invasion and population persistence within the ecosystem. Section 6 investigates how variation in reproduction and starvation rates influences the system's dynamics, including transitions between stability and extinction. Section 7 presents a sensitivity analysis to identify which parameters most significantly affect model outcomes. Finally, Section 8 explores how the model captures Cope's rule, illustrating how increased fat reserves may favor larger body sizes through enhanced competitive and energetic advantages.

2. Model parameters and biological interpretation

Understanding the ecological meaning and functional roles of model parameters is essential for interpreting the behavior of the starvation-recovery system. Each parameter in the NSM model encapsulates a distinct biological process—such as reproduction, starvation, mortality, or resource regeneration—and influences system stability in different ways. The balance among these processes determines whether the consumer-resource system can persist, oscillate, or collapse. Small changes in certain parameters can shift the system from sustainable coexistence to extinction. In this section, we systematically describe the biological interpretation of each parameter and discuss its effects when varied individually. The NSM model involves several parameters that govern the dynamics of full consumers (F), hungry consumers (H), and resources (R). Each parameter encapsulates a distinct ecological process, and its value critically affects system behavior, including potential extinction or persistence. Below, we provide the biological interpretation of each parameter and discuss its impact on system stability, as shown in Table 1.

Table 1. Model parameters with their biological roles and impact on system dynamics.

Param.	Biological role	If too high	If too low
λ	Reproduction rate of full consumers (F)	Population overshoot; instability	Insufficient growth; extinction risk
σ	Starvation rate: $F \to H$ when R is low	Rapid starvation; loss of F	Delayed response to resource shortage
μ	Mortality rate of hungry consumers (H)	Quick die-off; loss of recovery capacity	Unrealistic survival of starving individuals
ξ	Conversion efficiency of R to F via H	Sudden recovery; overgrowth risk	Poor recovery even with resources
ρ	Feeding rate of H on R	Resource collapse due to overfeeding	Ineffective use of available resources
δ	Baseline resource drain by H (maintenance)	Resource loss without recovery	Unrealistic maintenance without cost
β	Resource consumption by F	Excessive depletion of R	No cost for reproduction; biologically implausible
α	Intrinsic resource growth rate	Resource overshoot; instability	Resource fails to replenish; leads to starvation

Each parameter must be calibrated carefully to reflect biologically plausible dynamics. For example, if the starvation rate σ exceeds the reproduction rate λ, the population is likely to collapse, as full consumers become hungry faster than they can reproduce. Similarly, a high maintenance cost δ can drain resources even when consumer populations are low, destabilizing the ecosystem.

To ensure persistence of the system, parameters must balance reproduction, starvation, recovery, mortality, and resource renewal. In later sections, we analyze how varying these parameters influences the equilibrium behavior and extinction risk in the system.

To identify the equilibrium points of the system described by Eqs (1.1a)–(1.1c), we set the time derivatives equal to zero and solve the resulting algebraic equations for the state variables, see [30].

$$\lambda F + \xi\rho RH - \sigma(1 - R)F = 0,$$

$$\sigma(1 - R)F - \xi\rho RH - \mu H = 0,$$

$$\alpha(1 - R)R - (\rho R + \delta)H - \beta F = 0.$$

By solving the above equations, we get three equilibrium points: two trivial points at $(F_1^*, H_1^*, R_1^*) = (0, 0, 0)$ and $(F_2^*, H_2^*, R_2^*) = (0, 0, 1)$, and one non-trivial, internal point at

$$(F_3^*, H_3^*, R_3^*),$$

where

$$F_3^* = \frac{(\sigma - \lambda)\alpha\mu^2(\mu + \xi\rho)}{A[\lambda\rho B + \mu\sigma(\beta\mu + \lambda(\delta + \rho))]}, \quad H_3^* = \frac{(\sigma - \lambda)\alpha\lambda^2\mu(\mu + \xi\rho)}{A[\lambda\rho B + \mu\sigma(\beta\mu + \lambda(\delta + \rho))]}, \quad R_3^* = \frac{(\sigma - \lambda)\mu}{A},$$

where $A = \lambda\xi\rho + \mu\sigma$ and $B = \beta\mu\xi + \delta\lambda\xi - \lambda\mu$.

3. Stability analysis of equilibrium points

Fixed point (0,0,0)

The trivial extinction fixed point $(F^*, H^*, R^*) = (0, 0, 0)$ is analyzed by evaluating the Jacobian matrix and its eigenvalues. The Jacobian matrix at this point is given as

$$J(0, 0, 0) = \begin{bmatrix} \lambda - \sigma & 0 & 0 \\ \sigma & -\mu & 0 \\ -\beta & -\delta & \alpha \end{bmatrix}.$$

The eigenvalues of this matrix are $\lambda_1 = \lambda - \sigma$, $\lambda_2 = -\mu$, and $\lambda_3 = \alpha$. For the point to be stable, all eigenvalues must have negative real parts. This condition translates to $\lambda_1 < 0$, which requires $\sigma > \lambda$; $\lambda_2 < 0$, which is satisfied if $\mu > 0$; and $\lambda_3 < 0$, which would require $\alpha < 0$. However, $\alpha < 0$ is biologically implausible as it would imply a negative resource growth rate, making $(0, 0, 0)$ generally unstable under realistic biological conditions.

Bifurcation analysis reveals that a bifurcation occurs when $\lambda_1 = 0$, or equivalently, when $\sigma = \lambda$. At this critical point, the system transitions in stability: for $\sigma < \lambda$, $\lambda_1 > 0$, rendering $(0, 0, 0)$ unstable, while for $\sigma > \lambda$, $\lambda_1 < 0$, potentially stabilizing $(0, 0, 0)$ if $\alpha < 0$, though this is unlikely in biological terms. This transition represents a saddle-node bifurcation at $\sigma = \lambda$, highlighting the critical role of the starvation rate (σ) in determining the stability of the trivial extinction point.

To visualize the bifurcation, the eigenvalues of the Jacobian can be plotted as functions of σ. Figure 2 shows the bifurcation analysis of the eigenvalues of the Jacobian matrix at the trivial extinction fixed point $(F^*, H^*, R^*) = (0, 0, 0)$, as a function of the starvation rate parameter σ. The figure illustrates the dynamics of the system at the bifurcation point ($\sigma = \lambda$), where the bifurcation occurs as $\lambda_1 = 0$. For $\sigma < \lambda$, the trivial fixed point $(0, 0, 0)$ is unstable ($\lambda_1 > 0$), representing extinction, while for $\sigma > \lambda$, $\lambda_1 < 0$, rendering the trivial fixed point stable along certain axes, provided other eigenvalues do not dominate instability.

Along specific dimensions, stability and instability vary: the constant negative eigenvalue $\lambda_2 = -\mu$ ensures stability for the "Hungry Consumers" (H), while the positive eigenvalue $\lambda_3 = \alpha$ implies persistent instability for "Resources" (R). Biologically, the system transitions from extinction at $\sigma < \lambda$ to potential coexistence or new equilibrium dynamics at $\sigma > \lambda$, emphasizing the critical role of the starvation rate (σ) in determining population outcomes. This represents a saddle-node bifurcation,

where the fixed point's stability shifts as λ_1 crosses zero, although the presence of a positive eigenvalue (λ_3) necessitates further analysis of non-trivial fixed points to fully understand population persistence. The figure thus captures the interplay of eigenvalues with σ, revealing the bifurcation point and its implications for system stability.

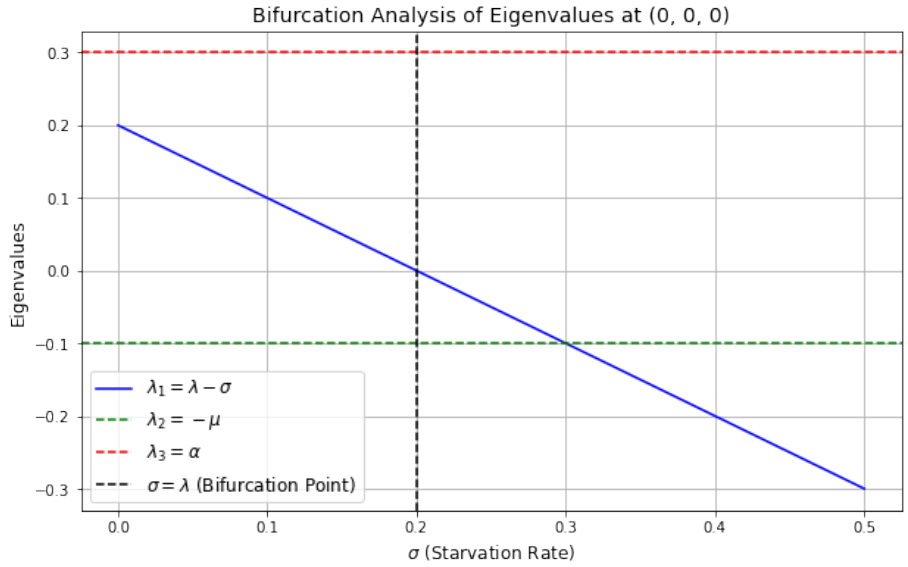

Figure 2. Bifurcation analysis of eigenvalues at $(0, 0, 0)$.

Fixed point $(0, 0, 1)$

The fixed point $(0, 0, 1)$ represents a scenario where resources are at their maximum capacity ($R = 1$) without any consumers present ($F = 0, H = 0$). The stability of this fixed point is analyzed using the Jacobian matrix, whose entries are derived from the partial derivatives of the system equations. Substituting $(F, H, R) = (0, 0, 1)$, the Jacobian simplifies to

$$J(0, 0, 1) = \begin{bmatrix} \lambda & \xi\rho & 0 \\ 0 & -\xi\rho - \mu & 0 \\ -\beta & -\rho - \delta & -\alpha \end{bmatrix}.$$

The eigenvalues of this matrix are $\lambda_1 = \lambda$, $\lambda_2 = -\xi\rho - \mu$, and $\lambda_3 = -\alpha$. For stability, all eigenvalues must have negative real parts. The first eigenvalue, $\lambda_1 = \lambda$, requires $\lambda < 0$; otherwise, the fixed point is unstable along the F-axis, leading to exponential growth of full consumers. The second eigenvalue, $\lambda_2 = -\xi\rho - \mu$, is negative for biologically plausible parameters ($\xi\rho + \mu > 0$), ensuring stability along the H-axis. The third eigenvalue, $\lambda_3 = -\alpha$, is negative if $\alpha > 0$, ensuring stability along the R-axis.

A bifurcation occurs when any eigenvalue crosses zero. For $\lambda_1 = \lambda$, a bifurcation arises at $\lambda = 0$, indicating a transition from stability ($\lambda < 0$) to instability ($\lambda > 0$) along the F-axis. The remaining eigenvalues, λ_2 and λ_3, remain constant and negative, preserving stability along the H- and R-axes.

A numerical example with parameters:

$$\lambda = 0.2, \quad \xi = 0.5, \quad \rho = 0.3, \quad \mu = 0.1, \quad \alpha = 0.3, \quad \beta = 0.1, \quad \delta = 0.2$$

yields the following eigenvalues:

$$\lambda_1 = 0.2, \quad \lambda_2 = -0.25, \quad \lambda_3 = -0.3,$$

confirming instability along the F-axis due to the positive eigenvalue $\lambda_1 > 0$.

Visualizing through bifurcation analysis reveals the dynamics of λ_1 as a function of λ, where it crosses zero at $\lambda = 0$. This bifurcation highlights the critical role of the reproduction rate in determining stability. Constant eigenvalues λ_2 and λ_3 ensure stability along the other axes, reflecting that the fixed point $(0, 0, 1)$ is unstable under realistic conditions when $\lambda > 0$.

Figure 3 illustrates the bifurcation dynamics for the fixed point $(0, 0, 1)$ as a function of the reproduction rate λ. The blue curve represents the eigenvalue $\lambda_1 = \lambda$, which crosses zero at $\lambda = 0$, marking the bifurcation point. For $\lambda > 0$, the fixed point becomes unstable along the F-axis, indicating exponential growth of full consumers. The green and red dashed lines correspond to the eigenvalues λ_2 and λ_3, respectively, which remain constant and negative, ensuring stability along the H- and R-axes. This bifurcation at $\lambda = 0$ underscores the critical role of the reproduction rate in determining system stability. Persistent instability along the F-axis, caused by $\lambda > 0$, prevents the fixed point $(0, 0, 1)$ from being globally stable under biologically realistic conditions.

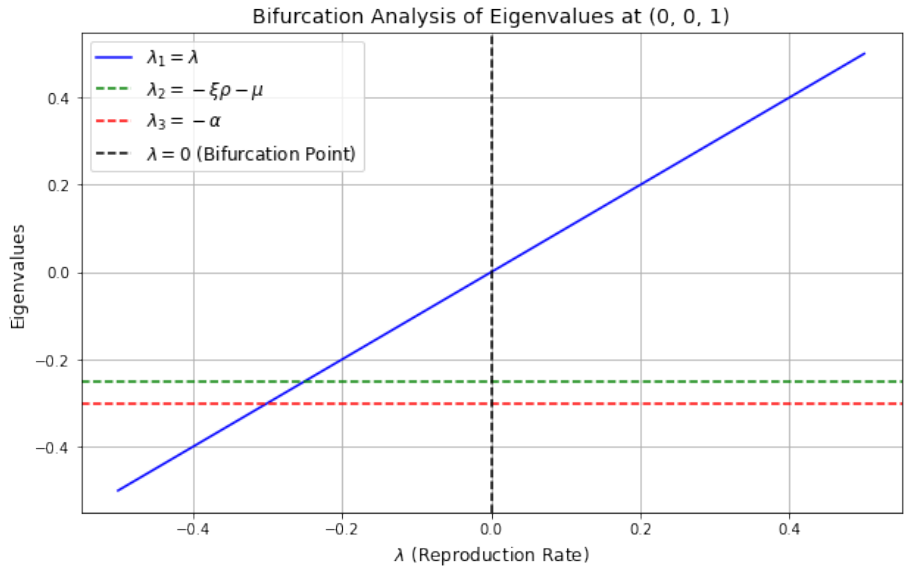

Figure 3. Bifurcation analysis of eigenvalues at (0,0,1).

Non-trivial fixed point

The non-trivial fixed point of the NSM is given by

$$F^* = \frac{(\sigma - \lambda)\alpha\mu^2(\mu + \xi\rho)}{A[\lambda\rho B + \mu\sigma(\beta\mu + \lambda(\delta + \rho))]}, \quad H^* = \frac{(\sigma - \lambda)\alpha\lambda^2\mu(\mu + \xi\rho)}{A[\lambda\rho B + \mu\sigma(\beta\mu + \lambda(\delta + \rho))]}, \quad R^* = \frac{(\sigma - \lambda)\mu}{A},$$

where $A = \lambda\xi\rho + \mu\sigma$ and $B = \beta\mu\xi + \delta\lambda\xi - \lambda\mu$. For the internal equilibrium (F_3^*, H_3^*, R_3^*) to be biologically meaningful, all components must be positive. From the expression $R_3^* = \frac{(\sigma-\lambda)\mu}{A}$ with $A = \lambda\xi\rho + \mu\sigma > 0$, it follows that $R_3^* > 0$ only if $\sigma > \lambda$. This condition ensures that starvation occurs at a sufficient rate to prevent unbounded population growth, allowing coexistence with the resource. Positivity of F_3^* and H_3^* further requires the denominator term $D = \lambda\rho B + \mu\sigma(\beta\mu + \lambda(\delta + \rho))$ to be positive. A sufficient condition for this is $B = \beta\mu\xi + \delta\lambda\xi - \lambda\mu > 0$, which implies that the combined effects of resource consumption and recovery efficiency dominate reproductive losses.

Stability analysis of this fixed point reveals that under typical ecological conditions, such as $\sigma > \lambda$, the real parts of all eigenvalues of the Jacobian matrix evaluated at (F^*, H^*, R^*) are negative. This ensures that the fixed point is globally stable, representing a state where consumers and resources coexist in a balanced equilibrium.

A bifurcation analysis highlights the occurrence of a transcritical bifurcation as σ approaches λ. From the expression for R^*, it follows immediately that the interior equilibrium is biologically feasible (all components positive) only when $\sigma > \lambda$. Moreover, since $R^* \propto (\sigma - \lambda)$, we have

$$R^* \to 0, \qquad F^* \to 0, \qquad H^* \to 0 \quad \text{as } \sigma \downarrow \lambda.$$

Thus at $\sigma = \lambda$ the interior positive branch coalesces with the extinction equilibrium $(0, 0, 0)$. This collision is accompanied by an eigenvalue crossing: the Jacobian at $(0, 0, 0)$ has eigenvalues $\lambda_1 = \lambda - \sigma$, $\lambda_2 = -\mu$, and $\lambda_3 = \alpha$, so λ_1 changes sign at $\sigma = \lambda$. The simultaneous facts that (i) the positive branch exists only for $\sigma > \lambda$, (ii) the branch limits to $(0, 0, 0)$ as $\sigma \downarrow \lambda$, and (iii) an eigenvalue of $(0, 0, 0)$ crosses zero at the same parameter value, are the characteristic ingredients of a *transcritical bifurcation*. Biologically, the threshold $\sigma = \lambda$ marks the critical balance between starvation and reproduction. When $\sigma < \lambda$ reproduction outpaces starvation and the interior equilibrium is not feasible, and when $\sigma > \lambda$ starvation sufficiently regulates reproduction, permitting a stable coexistence equilibrium. Therefore, the fact that $H_3^* = R_3^* = 0$ at $\sigma = \lambda$ is not unreasonable but is the expected signature of this transcritical exchange of stability. For a numerical example with parameter values $\lambda = 0.2$, $\xi = 0.5$, $\rho = 0.3$, $\mu = 0.1$, $\alpha = 0.4$, $\delta = 0.2$, $\beta = 0.1$, and $\sigma = 0.25$, the fixed point is computed as

$$F^* \approx 0.0162, \quad H^* \approx 0.0096, \quad R^* \approx 0.5.$$

Stability analysis of the Jacobian matrix at this fixed point confirms that all eigenvalues have negative real parts, affirming stability for $\sigma > \lambda$. This analysis demonstrates the model's ability to describe stable coexistence and highlights the critical role of bifurcation in transitions between extinction and coexistence.

Figure 4 represents the bifurcation analysis of the non-trivial internal fixed point (F^*, H^*, R^*), showing how the fixed point components F^*, H^*, and R^* depend on the starvation rate parameter σ. For starvation rates below λ, i.e., before $\sigma = \lambda$ ($\sigma < \lambda$), F^*, H^*, and R^* have negative or undefined values. This indicates that the fixed point is not biologically feasible due to negative population or resource densities. At $\sigma = \lambda$, the curves for F^*, H^*, and R^* approach zero. This represents a **transcritical bifurcation**, where the non-trivial fixed point merges with the trivial fixed point $(0, 0, 0)$. The system transitions between extinction ($(0, 0, 0)$) and coexistence ($(F^*, H^*, R^*) > 0$).

For starvation rates above λ, i.e., after $\sigma = \lambda$ ($\sigma > \lambda$), F^* (full consumers) increases steadily as σ grows. H^* (hungry consumers) also increases but at a slower rate than F^*. R^* (resource availability) stabilizes at a moderate value and remains positive. This indicates that the populations coexist with a stable resource base when σ exceeds the critical threshold.

The dashed line ($\sigma = \lambda$) marks the bifurcation point. Below this point, the non-trivial fixed point is not feasible, while above this point, the populations and resources stabilize at positive values. For $\sigma > \lambda$, the ecosystem reaches a stable equilibrium where full and hungry consumers coexist with a sustainable level of resources. For $\sigma \leq \lambda$, the system collapses to extinction as populations and resources cannot coexist. A higher starvation rate leads to more full and hungry consumers as σ

increases beyond λ. Resource availability (R^*) stabilizes, indicating a balance between consumption and replenishment.

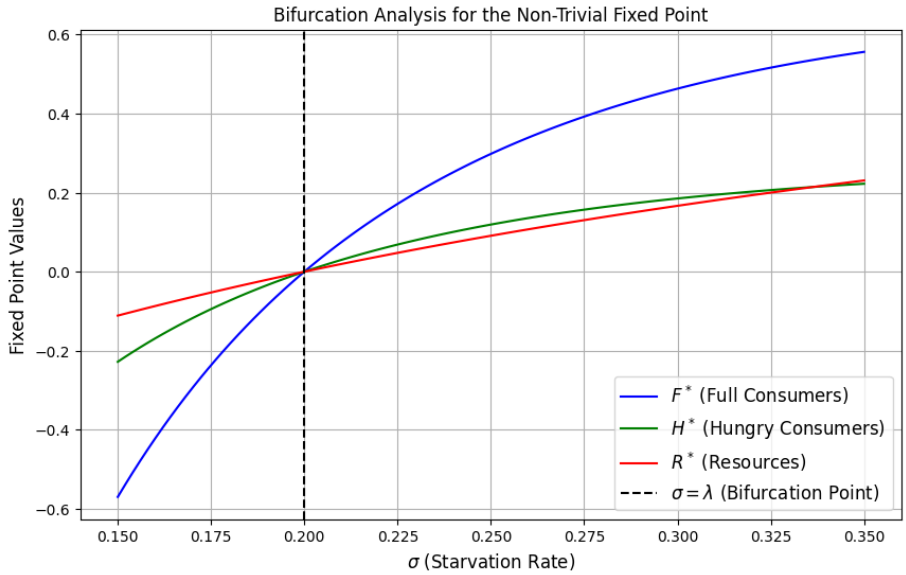

Figure 4. Bifurcation analysis for the non-trivial fixed point.

4. Dissipativeness and persistence

In this section, we analyze the dissipativeness and persistence of the consumer-resource system defined by Eqs (1.1), which describe the dynamics of full consumers (F), hungry consumers (H), and resources (R). Dissipativeness ensures that all solutions are ultimately bounded, while persistence implies the long-term survival of all populations, preventing solutions from approaching the boundary of the non-negative cone $\mathbb{R}^3_+$.

Definition 4.1 (Dissipativeness)**.** *System* (1.1) *is said to be* dissipative *if there exists a compact absorbing set* $B \subset \mathbb{R}^3_+$ *such that every solution* $(F(t), H(t), R(t))$ *with an initial condition in* $\mathbb{R}^3_+ \setminus \{0\}$ *eventually enters* B *and remains in it for all sufficiently large* t.

Theorem 4.1 (Uniform boundedness of solutions)**.** *Let all parameters in system* (1.1) *be strictly positive. Then every solution with an initial condition in* $\mathbb{R}^3_+ \setminus \{0\}$ *is uniformly bounded, and the system is dissipative.*

Proof. Define the Lyapunov-like functional

$$\Sigma(t) = F(t) + H(t) + cR(t),$$

for some constant $c > 0$. Differentiating with respect to time gives

$$\frac{d\Sigma}{dt} = \dot{F} + \dot{H} + c\dot{R},$$

and substituting from system (1.1):

$$\begin{aligned}\frac{d\Sigma}{dt} &= (\lambda F + \xi\rho RH - \sigma(1-R)F) + (\sigma(1-R)F - \xi\rho RH - \mu H) \\ &\quad + c\left(\alpha(1-R)R - (\rho R + \delta)H - \beta F\right).\end{aligned}$$

Simplifying, we get

$$\frac{d\Sigma}{dt} = F\left(\lambda - \sigma(1-R) - c\beta\right) - H\left(\mu + c(\rho R + \delta)\right) + c\alpha R(1-R).$$

Note that $R(1-R) \leq \frac{1}{4}$ for $R \in [0,1]$. Choose

$$c \geq \frac{\lambda + \sigma}{\beta},$$

so that

$$\lambda - \sigma(1-R) - c\beta \leq \lambda + \sigma - c\beta \leq 0.$$

Hence, the F-term is nonpositive. The H-term is strictly negative, and the last term is bounded above by $\frac{c\alpha}{4}$. Thus,

$$\frac{d\Sigma}{dt} \leq \frac{c\alpha}{4}.$$

We now apply a differential inequality of the form

$$\frac{d\Sigma}{dt} + \mu'\Sigma \leq \frac{c\alpha}{4}$$

for $\mu' := \min\{\mu, \beta c\} > 0$. Solving this linear inequality using the integrating factor method (or Gronwall's inequality), we obtain

$$\Sigma(t) \leq \Sigma(0)e^{-\mu' t} + \frac{c\alpha}{4\mu'}\left(1 - e^{-\mu' t}\right).$$

Taking $t \to \infty$, we conclude

$$\limsup_{t\to\infty} \Sigma(t) \leq \frac{c\alpha}{4\mu'}.$$

Therefore, for any $\varepsilon > 0$, there exists $T > 0$ such that for all $t > T$:

$$F(t) + H(t) + cR(t) \leq \frac{c\alpha}{4\mu'} + \varepsilon.$$

Define the absorbing set

$$\mathcal{B} = \left\{(F, H, R) \in \mathbb{R}^3_+ \,\middle|\, F + H + cR \leq \frac{c\alpha}{4\mu'} + \varepsilon\right\},$$

which is compact in $\mathbb{R}^3_+$. Since all trajectories eventually enter and remain in $\mathcal{B}$, the system is dissipative.

Furthermore, note that

- $\dot{R} < 0$ for $R > 1$,
- $\dot{F}, \dot{H}, \dot{R} \geq 0$ at the coordinate planes $F = 0$, $H = 0$, $R = 0$.

So trajectories remain in the positive orthant and are forward-invariant. □

Definition 4.2 (Persistence)**.** *System* (1.1) *is said to be* persistent *if for all initial conditions* $(F(0), H(0), R(0)) \in \mathbb{R}^3_+ \setminus \{0\}$*, the corresponding solution satisfies:*

$$\liminf_{t\to\infty} F(t) > 0, \quad \liminf_{t\to\infty} H(t) > 0, \quad \liminf_{t\to\infty} R(t) > 0.$$

That is, no omega-limit points lie on the boundary of $\mathbb{R}^3_+$*; all components of the state vector persist over time.*

Theorem 4.2 (Persistence of the eco-evolutionary system)**.** *Suppose the parameters satisfy* $\lambda, \xi, \rho, \sigma, \mu, \alpha, \delta, \beta > 0$*, and system is initiated with* $(F(0), H(0), R(0)) \in \mathbb{R}^3_+ \setminus \{0\}$*. Then system* (1.1) *is persistent. That is, the positive orthant is forward invariant and repelling on all boundary planes.*

Proof. We examine dynamics on the boundary of $\mathbb{R}^3_+$ to verify that no trajectory can remain on or asymptotically approach the boundary unless it converges to the origin. We consider each coordinate plane separately as

(i) Boundary $F = 0$

$$\dot{F} = \xi\rho RH.$$

If $R > 0$ and $H > 0$, then $\dot{F} > 0$, so trajectories leave the boundary. If $R = 0$ or $H = 0$, we analyze

$$\dot{H} = -(\xi\rho R + \mu)H \leq 0, \quad \dot{R} = \alpha(1 - R)R - (\rho R + \delta)H.$$

At the corner point $(0, 0, 0)$, $\dot{R} = 0$, but in any neighborhood with $R > 0$, $\dot{R} \approx \alpha R > 0$, so solutions escape the origin. At $(0, 0, 1)$, we have

$$\dot{F} = 0, \quad \dot{H} = -(\xi\rho + \mu)H, \quad \text{but } \left.\frac{\partial \dot{F}}{\partial F}\right|_{(0,0,1)} = \lambda > 0.$$

Hence, the boundary is transversally unstable.

(ii) Boundary $H = 0$

$$\dot{H} = \sigma(1 - R)F.$$

If $F > 0$ and $R < 1$, then $\dot{H} > 0$, repelling solutions from the boundary. If $R = 1$, then $\dot{H} = 0$, but

$$\dot{F} = \lambda F > 0, \quad \dot{R} = -\beta F < 0,$$

so R decreases and $\dot{H}$ becomes positive. At $(0, 0, 1)$, as before, $\frac{\partial \dot{H}}{\partial H} > 0$ due to positive λ, so solutions cannot remain at $H = 0$.

(iii) Boundary $R = 0$

$$\dot{R} = -\delta H - \beta F.$$

At first glance, this suggests $\dot{R} \leq 0$. However, if $F = H = 0$, then $\dot{R} = 0$, and for small $R > 0$, the logistic term dominates

$$\dot{R} = \alpha(1 - R)R \approx \alpha R > 0.$$

Thus, $R = 0$ is not attracting. If $F > 0$ or $H > 0$, then $\dot{R} < 0$, but the boundedness of $R(t) \geq 0$ ensures solutions cannot stay at $R = 0$.

(iv) Corner point $(0, 0, 0)$

At the origin

$$\dot{F} = 0, \quad \dot{H} = 0, \quad \dot{R} = 0,$$

but for any small perturbation $R > 0$, $\dot{R} = \alpha R > 0$, and the system leaves the origin. Thus, the origin is non-attracting.

Since all boundaries are repelling, and the system is dissipative (trajectories are uniformly bounded due to resource saturation and consumer mortality), the positive orthant is invariant and solutions are repelled from the boundary. Hence, the system is persistent. □

The basic reproduction number $\mathcal{R}_0$ quantifies the expected number of new full consumers produced by a single full consumer introduced into a resource-abundant environment. It provides a threshold for the invasion potential of the consumer population in the eco-evolutionary model (1.1), indicating whether the consumer population can successfully establish and grow when initially rare; for more details, see [8]. In the context of the NSM, $\mathcal{R}_e$ represents an *ecological analogue* of the reproduction number. It defines the threshold between population extinction and persistence, indicating whether a small group of full consumers can successfully invade and maintain a stable presence within an unexploited resource environment.

5. Invasion and persistence threshold $\mathcal{R}_e$ ($\mathcal{R}_0$ analogue)

To evaluate $\mathcal{R}_e$, we analyze the system at the *consumer-free equilibrium* $(F^*, H^*, R^*) = (0, 0, 1)$, where both full and hungry consumers are absent, and the resource is at its maximum carrying capacity. This equilibrium represents the worst-case scenario for resistance to invasion—resources are plentiful and unexploited, so even minimal reproductive success could allow consumers to invade. Mathematically, this point corresponds to the boundary equilibrium where consumer equations can be linearized and analyzed using the next-generation matrix method. Biologically, it captures the state of an undisturbed ecosystem prior to consumer colonization.

Theorem 5.1. *Let the eco-evolutionary model* (1.1) *incorporate a natural mortality rate $m > 0$ for full consumers. Then, the analogue of the basic reproduction number is given by*

$$\mathcal{R}_e = \frac{\lambda}{m},$$

where λ is the reproduction rate of full consumers. The consumer-free equilibrium is locally asymptotically stable if $\mathcal{R}_e < 1$ and unstable if $\mathcal{R}_e > 1$.

Proof. To compute $\mathcal{R}_e$, we use the next-generation matrix method. Let $X = [F, H]^T$, and decompose the dynamics into "new infections" $\mathcal{F}(X)$ and "transitions" $\mathcal{V}(X)$ as

$$\dot{X} = \mathcal{F}(X) - \mathcal{V}(X).$$

From the modified system with full consumer mortality m, we have

$$\mathcal{F} = \begin{bmatrix} \lambda F + \xi\rho RH \\ \sigma(1-R)F \end{bmatrix}, \quad \mathcal{V} = \begin{bmatrix} (m + \sigma(1-R))F \\ \xi\rho RH + \mu H \end{bmatrix}.$$

Evaluating the Jacobians at the consumer-free equilibrium $(F, H, R) = (0, 0, 1)$, we obtain

$$f = \left.\frac{\partial \mathcal{F}}{\partial(F,H)}\right|_{(0,0,1)} = \begin{bmatrix} \lambda & \xi\rho \\ 0 & 0 \end{bmatrix}, \quad v = \left.\frac{\partial \mathcal{V}}{\partial(F,H)}\right|_{(0,0,1)} = \begin{bmatrix} m & 0 \\ 0 & \xi\rho + \mu \end{bmatrix}.$$

Then the next-generation matrix is

$$G = fv^{-1} = \begin{bmatrix} \frac{\lambda}{m} & \frac{\xi\rho}{\xi\rho+\mu} \\ 0 & 0 \end{bmatrix}.$$

The basic reproduction number is the spectral radius of G, i.e.,

$$\mathcal{R}_e = \rho(G) = \frac{\lambda}{m}.$$

Thus, $\mathcal{R}_e > 1$ implies exponential growth of the full consumer population, while $\mathcal{R}_e < 1$ implies decay. □

Remark. If the natural mortality of full consumers is neglected ($m = 0$), the reproduction number becomes infinite:

$$\mathcal{R}_e = \infty,$$

which reflects unrealistic unbounded growth. This corresponds to an epidemic without recovery or death. Introducing mortality regularizes the invasion threshold and parallels epidemiological models such as SIR and SEIR, where a finite $\mathcal{R}_0$ governs outbreak potential.

6. Impact of reproduction and starvation rates on system dynamics

To investigate the eco-evolutionary consequences of the balance between reproduction and starvation, we consider two distinct parameter regimes: one where the starvation rate dominates reproduction ($\sigma > \lambda$), and another where reproduction dominates starvation ($\lambda > \sigma$). Specifically, we simulate the system dynamics under the following parameter sets:

- **Case 1 (Starvation dominant)**: $\lambda = 0.5\ \mathrm{s}^{-1}$, $\sigma = 1.5\ \mathrm{s}^{-1}$;
- **Case 2 (Reproduction dominant)**: $\lambda = 1.5\ \mathrm{s}^{-1}$, $\sigma = 0.5\ \mathrm{s}^{-1}$.

All other parameters are held constant across both cases:

$$\xi = 0.6 \text{ (dimensionless)}, \quad \rho = 0.5\ \mathrm{s}^{-1}, \quad \mu = 0.1\ \mathrm{s}^{-1}, \quad \alpha = 1.0\ \mathrm{s}^{-1}, \quad \delta = 0.05\ \mathrm{s}^{-1}, \quad \beta = 0.02\ \mathrm{s}^{-1}.$$

Initial conditions for both simulations are:

$$F_0 = 0.2 \text{ (dimensionless)}, \quad H_0 = 0.1 \text{ (dimensionless)}, \quad R_0 = 0.5 \text{ (dimensionless)},$$

with simulations run over the time interval $t \in [0, 10]$ s.

Case 1: Starvation rate $\sigma > \lambda$

As shown in Figure 5, when starvation significantly exceeds reproduction ($\sigma = 1.5\ s^{-1}$, $\lambda = 0.5\ s^{-1}$), the system evolves to a state where most individuals are driven into the hungry non-reproducing state. The full consumer population remains low throughout the simulation due to high transition rates from full to hungry consumers. Consequently, reproduction is suppressed, resulting in a low total consumer density. However, since consumer pressure on the resource is diminished, the resource level stabilizes at a relatively high value.

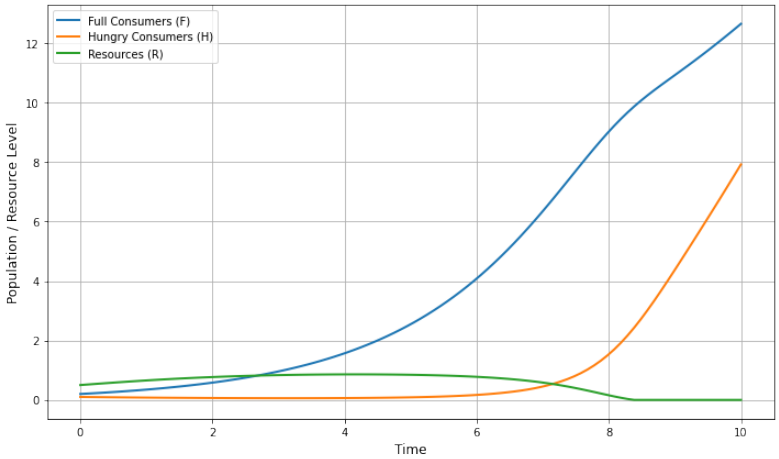

Figure 5. Time evolution of consumer-resource dynamics under high a starvation rate ($\sigma = 1.5\ s^{-1}$, $\lambda = 0.5\ s^{-1}$).

Case 2: Reproduction rate $\lambda > \sigma$

Figure 6 illustrates the system dynamics when the reproduction rate exceeds starvation ($\lambda = 1.5\ s^{-1}$, $\sigma = 0.5\ s^{-1}$). In this regime, full consumers rapidly increase due to enhanced reproduction and reduced starvation transitions. The population of hungry consumers also rises as more individuals cycle through the states. However, the elevated consumer density exerts heavy pressure on the resource base, leading to rapid depletion. The system exhibits large transient oscillations in both consumer and resource populations, highlighting potential instability due to overexploitation.

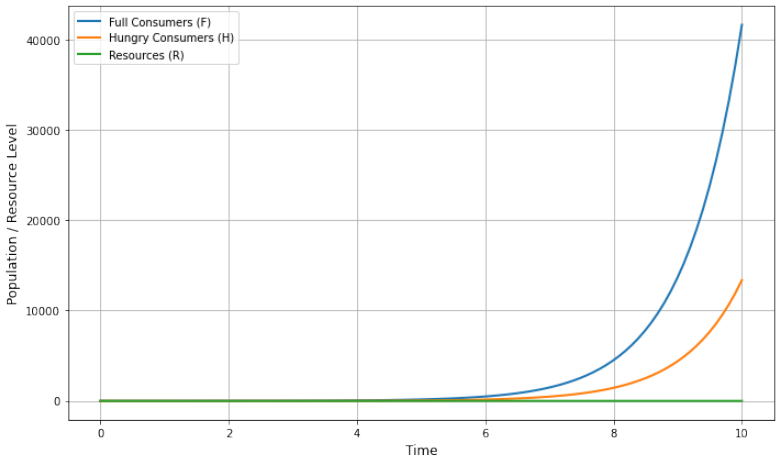

Figure 6. Time evolution of consumer-resource dynamics under a high reproduction rate ($\lambda = 1.5\ s^{-1}$, $\sigma = 0.5\ s^{-1}$).

These simulations demonstrate that a high starvation rate suppresses consumer density and stabilizes resource levels, but at the cost of reproductive output. In contrast, when reproduction dominates starvation, the consumer population grows rapidly, potentially overshooting resource availability and inducing oscillatory dynamics. These results highlight the delicate balance between energy acquisition, reproductive strategy, and starvation tolerance in shaping ecological stability.

7. Parameter sensitivity analysis

To investigate the eco-evolutionary dynamics captured by the starvation-recovery model, we systematically varied key parameters and analyzed their influence on the temporal evolution of full consumers (F), hungry consumers (H), and resources (R). The system's dynamics are governed by the set of differential equations described in (1.1). Unless otherwise stated, the default parameter values used in the simulations are listed in Table 2.

Table 2. Default parameter values, corresponding units, and the specific values varied in the numerical simulations for time $T = 20$.

Parameter	Default value	Units	Values used in simulations
λ	0.4	s^{-1}	0.2, 0.4, 0.6, 0.8
σ	0.3	s^{-1}	0.1, 0.3, 0.5, 0.7
μ	0.1	s^{-1}	fixed
α	1.0	s^{-1}	fixed
β	0.05	s^{-1}	fixed
δ	0.05	s^{-1}	fixed
ρ	1.0	s^{-1}	0.5, 1.0, 1.5, 2.0
ξ	1.0	dimensionless	fixed

Effect of reproduction rate (λ)

Figure 7 illustrates the sensitivity of the system to the reproduction rate of full consumers, λ. As λ increases, the growth of the full consumer population (F) becomes exponential (Figure 7(a)), driven by the positive feedback from reproduction. This rapid expansion, however, accelerates resource depletion (Figure 7(b)), leading to a collapse of the resource base. The depletion of R subsequently triggers an increase in the hungry consumer population (H) (Figure 7(c)), as more individuals transition from F to H due to starvation in the absence of adequate resources. Notably, the overexploitation of resources at higher λ values induces oscillatory or collapse-prone dynamics, underscoring the ecological cost of aggressive reproductive strategies.

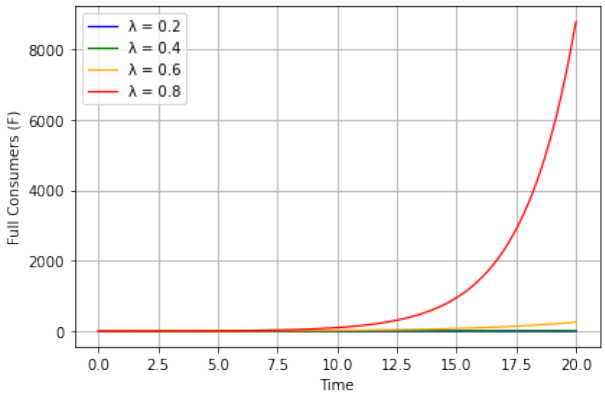

(**a**) Effect of λ on F

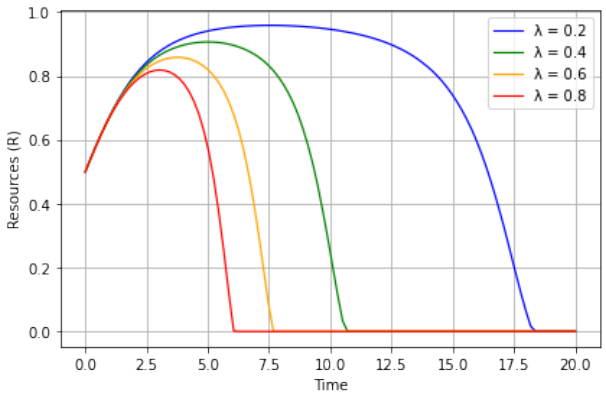

(**b**) Effect of λ on R

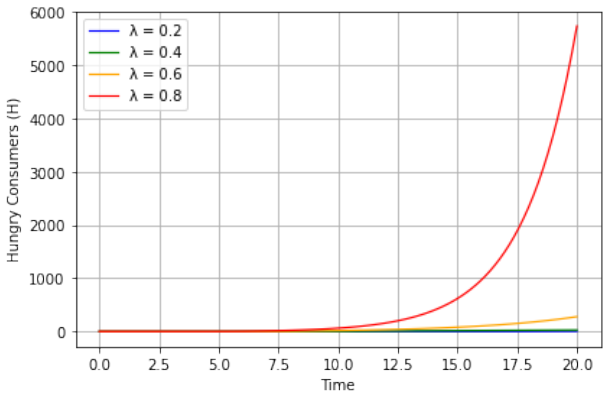

(**c**) Effect of λ on H

Figure 7. Parameter sensitivity: effect of λ.

Effect of starvation rate (σ)

In contrast, Figure 8 examines the role of the starvation rate σ, which governs the rate at which full consumers transition to the hungry state under resource scarcity. Increasing σ results in a marked decline in the full consumer population (Figure 8(a)) and a moderate rise in hungry consumers (Figure 8(c)). Since hungry individuals are less efficient at reproduction and recovery, this leads to slower overall population growth. The rapid conversion of F to H limits consumer pressure on resources, thereby delaying the collapse of R (Figure 8(b)). This suggests that higher σ acts as a stabilizing force in the system, preventing overexploitation by curbing the proliferation of full consumers.

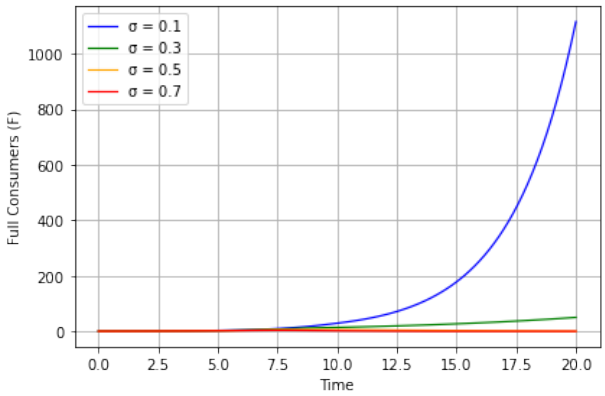

(**a**) Effect of σ on F

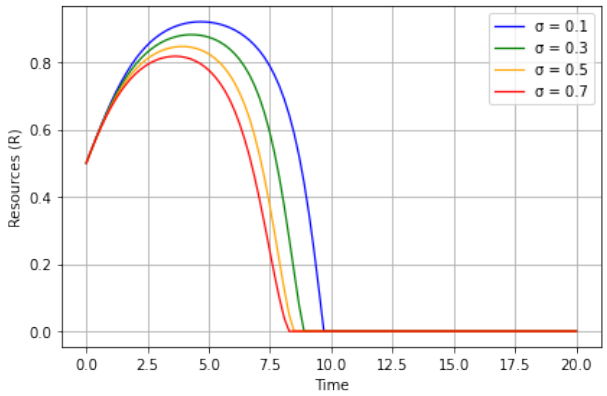

(**b**) Effect of σ on R

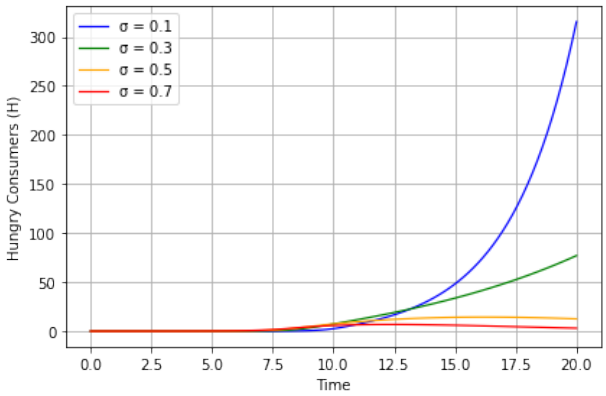

(**c**) Effect of σ on H

Figure 8. Parameter sensitivity: effect of σ.

Effect of consumption efficiency (ρ)

Finally, Figure 9 explores the effect of varying the resource consumption efficiency ρ, which modulates both the recovery of hungry consumers and the depletion of resources. Interestingly, higher values of ρ slow down the growth of both F and H populations (Figures 9(a) and (c)), primarily due to accelerated resource exhaustion. As ρ increases, hungry consumers recover more efficiently to the full state, but this comes at the cost of faster resource depletion (Figure 9(b)), leading to an earlier onset of starvation. Lower ρ values, on the other hand, produce more gradual dynamics and prolonged resource availability. These findings highlight a trade-off between short-term recovery benefits and long-term ecological sustainability, governed by how efficiently consumers utilize available resources.

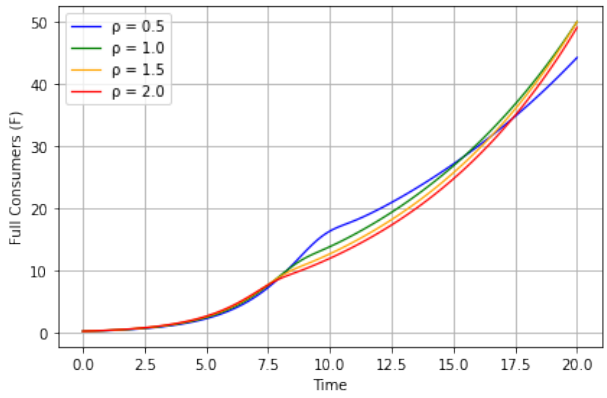

(**a**) Effect of ρ on F

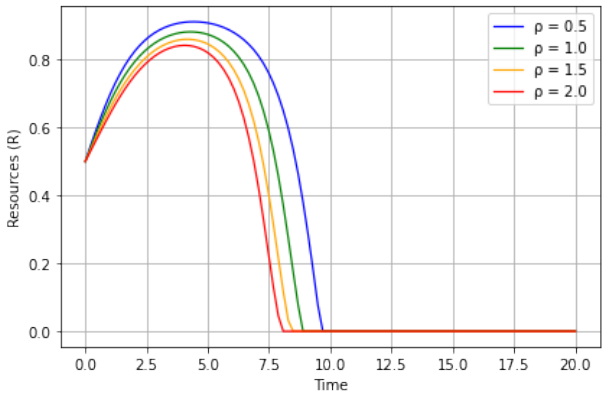

(**b**) Effect of ρ on R

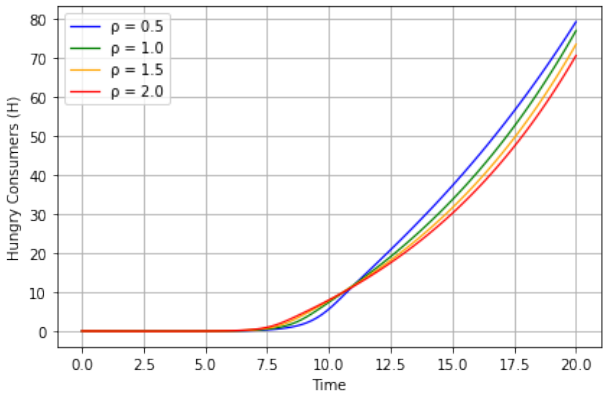

(**c**) Effect of ρ on H

Figure 9. Parameter sensitivity: effect of ρ.

To investigate how key ecological processes shape the internal dynamics of the NSM model, we perform a parametric sensitivity analysis of the non-trivial equilibrium point (F_3^*, H_3^*, R_3^*) with respect to the reproduction rate λ and the starvation rate σ, which govern the growth of full consumers and their transition to the hungry state, respectively, under the condition when $\sigma > \lambda$. Using 3D surface plots, we visualize the equilibrium values of full consumers, hungry consumers, and the resource across a biologically plausible range of $\lambda \in [0.01, 0.49]$ and $\sigma \in [0.5, 1.5]$, while holding all other parameters constant: intrinsic resource growth rate $\alpha = 0.5\ \text{s}^{-1}$, mortality rate of hungry consumers $\mu = 0.2\ \text{s}^{-1}$, resource-to-consumer conversion efficiency $\xi = 0.3$, feeding rate $\rho = 0.4\ \text{s}^{-1}$, baseline resource drain $\delta = 0.1\ \text{s}^{-1}$, and consumption rate by full consumers $\beta = 0.1\ \text{s}^{-1}$. The resulting Figure 10 reveals that F_3^* (full consumers) is highest when both reproduction and starvation are low, while H_3^* (hungry consumers) increases under high starvation and low reproduction, indicating energy imbalance. Conversely, R_3^* (resource level) increases with higher starvation and decreases with higher reproduction, reflecting reduced consumer pressure under resource scarcity. Ecologically, these results highlight the need for a delicate balance between consumer growth and starvation response: excessive reproduction or insufficient starvation may lead to resource collapse, while overly rapid starvation impedes population recovery— ultimately destabilizing the system.

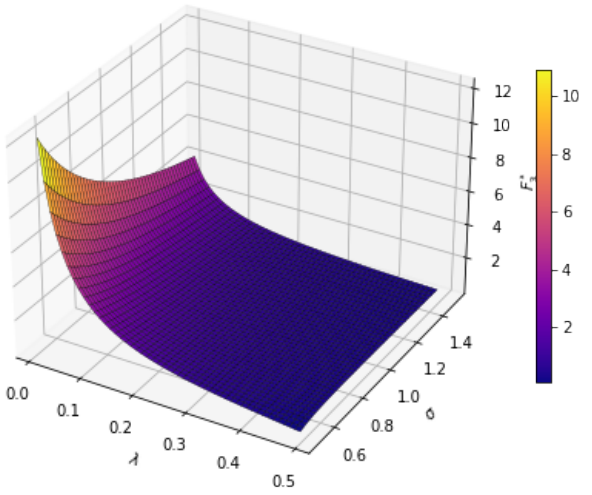

(**a**) F_3^*: Equilibrium density of full consumers.

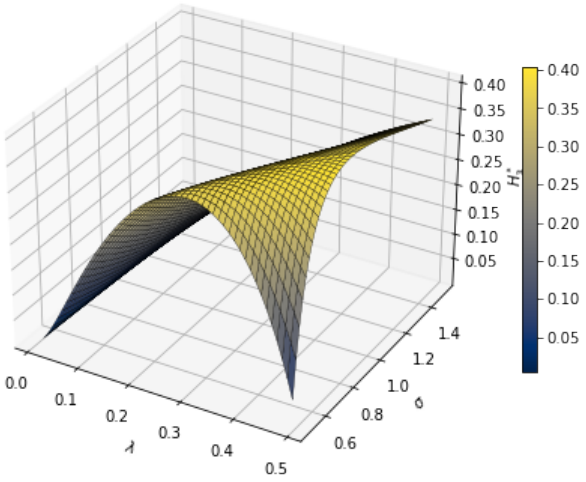

(**b**) H_3^*: Equilibrium density of hungry consumers.

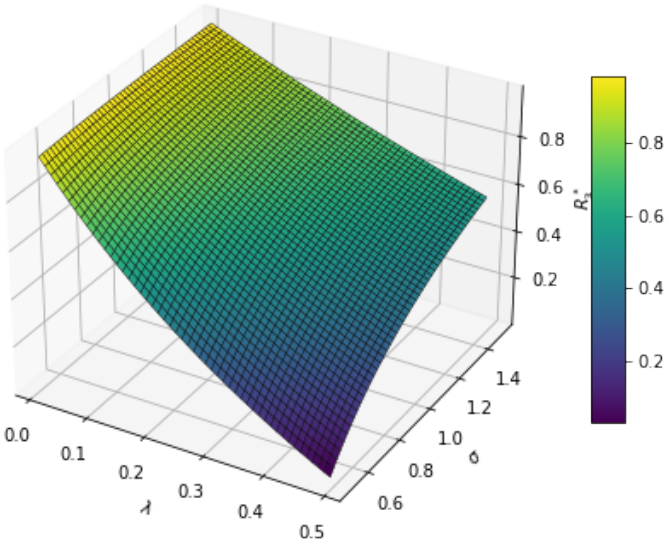

(**c**) R_3^*: Equilibrium level of the resource.

Figure 10. 3D surface plots of the non-trivial equilibrium point (F_3^*, H_3^*, R_3^*) as functions of reproduction rate λ and starvation rate σ with $\sigma > \lambda$.

Next, we visualize the internal equilibrium values (F_3^*, H_3^*, R_3^*) in the collapse regime defined by $\lambda > \sigma$, where reproduction outpaces starvation. The parameter ranges explored are $\lambda \in [0.5, 1.5]$ and $\sigma \in [0.01, 0.49]$, ensuring the system operates below the critical bifurcation line $\sigma = \lambda$. The first plot (Figure 11a) shows the equilibrium density of full consumers (F_3^*), which drops sharply or becomes undefined as the system destabilizes. Similarly, the second plot (Figure 11b) for hungry consumers (H_3^*) exhibits extreme values and non-biological behavior, indicating that the population cannot persist under these energetic imbalances. The third plot (Figure 11c) presents the equilibrium resource level

(R_3^*), which becomes negative across most of the domain, reflecting complete overexploitation of the resource. Together, the plots in Figure 11 confirm that when reproduction exceeds starvation (i.e., $\lambda > \sigma$), the NSM predicts ecological collapse characterized by unsustainable consumer densities and depleted resources.

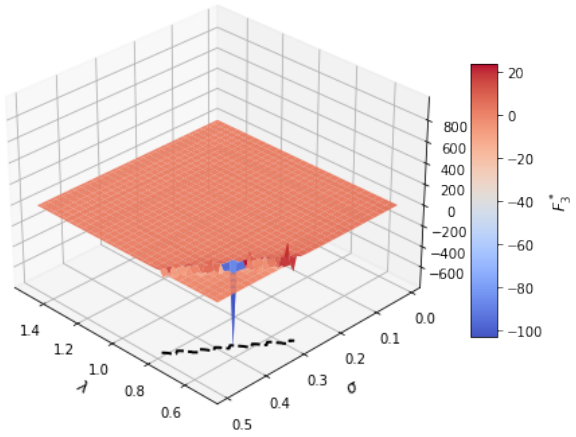

(**a**) F_3^*: Equilibrium density of full consumers.

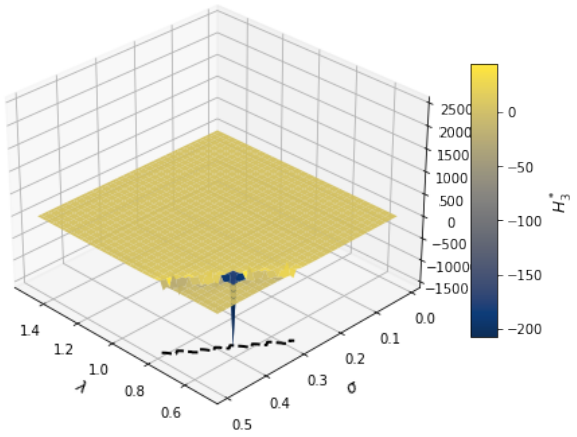

(**b**) H_3^*: Equilibrium density of "hungry" consumers.

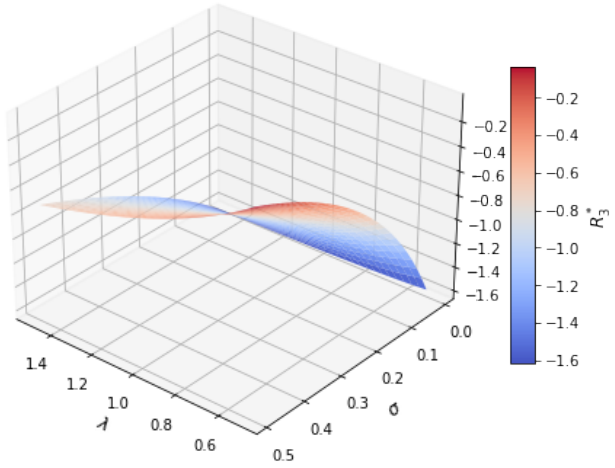

(**c**) R_3^*: Equilibrium level of the resource.

Figure 11. Equilibrium outcomes (F_3^*, H_3^*, R_3^*) of the model under the collapse regime where $\lambda > \sigma$.

8. Cope's rule in the nutritional state-structured model

Cope's rule posits that evolutionary lineages tend to increase in body size over time, a pattern widely observed in mammalian fossil records. By incorporating allometric scaling and body fat reserves, the NSM demonstrates that larger body sizes and higher fat reserves confer a selective advantage through reduced starvation rates, lower extinction risk, and competitive superiority, driving the evolutionary

trend toward larger body sizes up to an optimal mass ($M_{\text{opt}} \approx 1.748 \times 10^7$ g) and an upper bound ($M_{\text{max}} = 6.54 \times 10^7$ g), see [30].

The non-trivial equilibrium (F_3^*, H_3^*, R_3^*) represents stable coexistence, critical for analyzing Cope's rule. The NSM supports Cope's rule through three mechanisms:

(1) **Reduced starvation rates**: Larger body sizes increase fat reserves, reducing σ, the rate at which full consumers become hungry, maintaining a higher proportion of reproductive individuals (F).

(2) **Lower extinction risk**: The model identifies a stable "refuge" region in σ vs. ρ parameter space, where extinction risk is minimized. Larger body sizes align with this region due to lower σ.

(3) **Competitive advantage**: Populations with higher fat reserves ($\chi > 0$) maintain lower R_3^* for body masses below $M_{\text{opt}} \approx 1.748 \times 10^7$ g, outcompeting leaner populations by sustaining populations at lower resource levels.

The model predicts an upper bound on terrestrial mammalian body size at $M_{\text{max}} = 6.54 \times 10^7$ g, where energetic reserves reach zero ($\epsilon_p = 0$), consistent with fossil evidence (e.g., *Indricotherium* at $\sim 1.5 \times 10^7$ g).

We evaluate the internal equilibrium (F_3^*, H_3^*, R_3^*) for body masses $M = 10^4$ g (e.g., a hare) and $M = 10^6$ g (e.g., a rhinoceros), with fat reserve levels $\chi = 0.1$ (high reserves) and $\chi = -0.1$ (low reserves). Parameters are derived from allometric scaling:

- **Reproduction rate**: $\lambda = 0.1M^{-3/4}$, so $\lambda = 0.01\,\text{yr}^{-1}$ ($M = 10^4$), $\lambda = 0.001\,\text{yr}^{-1}$ ($M = 10^6$).
- **Starvation rate**: $\sigma = 0.05M^{-1/4}$, so $\sigma = 0.0158\,\text{yr}^{-1}$ ($M = 10^4$), $\sigma = 0.0089\,\text{yr}^{-1}$ ($M = 10^6$). For $\chi = 0.1$, reduce σ by 10% ($\sigma = 0.0142, 0.0080$); for $\chi = -0.1$, increase by 10% ($\sigma = 0.0174, 0.0098$).
- **Recovery rate**: $\rho = 0.1M^{-1/4}$, so $\rho = 0.0316\,\text{yr}^{-1}$ ($M = 10^4$), $\rho = 0.0178\,\text{yr}^{-1}$ ($M = 10^6$). For $\chi = 0.1$, increase ρ by 10% ($\rho = 0.0348, 0.0196$); for $\chi = -0.1$, decrease by 10% ($\rho = 0.0284, 0.0160$).
- **Other parameters**: $\mu = 0.1\,\text{yr}^{-1}$, $\xi = 1$, $\alpha = 1\,\text{yr}^{-1}$, $\delta = 0.01$, $\beta = 0.01$.

Using the equilibrium formulas, we calculate

$$F_3^* \approx 100.4, \quad H_3^* \approx 0.00100.$$

Higher fat reserves ($\chi = 0.1$) yield lower R_3^* (0.237 vs. 0.366 for $M = 10^4$, 0.854 vs. 0.892 for $M = 10^6$), indicating a competitive advantage. For $M = 10^4$, higher fat reserves increase F_3^* but reduce H_3^*, reflecting lower starvation flux. For $M = 10^6$, lower σ and λ reduce H_3^*, stabilizing populations.

Extinction risk is defined as the population falling below 20% of steady-state density ($F_3^* + H_3^*$). We calculate the proportion of full consumers:

$$\frac{F_3^*}{F_3^* + H_3^*} = \frac{1}{1 + \frac{\lambda^2}{\mu^2}}.$$

- $M = 10^4$ ($\lambda = 0.01, \mu = 0.1$): $\frac{F_3^*}{F_3^* + H_3^*} \approx 0.990$.

- $M = 10^6$ ($\lambda = 0.001, \mu = 0.1$): $\frac{F_3^*}{F_3^*+H_3^*} \approx 0.999$.

Larger body sizes increase the proportion of full consumers, reducing extinction risk. We simulate the system using the Euler method ($F(0) = 0.5$, $H(0) = 0.2$, $R(0) = 0.8$, $\Delta t = 0.01$, 1000 years, 100 runs with $\alpha \in [0.9, 1.1]$). Extinction probabilities:

- $M = 10^4, \chi = 0.1$: ~4%.
- $M = 10^4, \chi = -0.1$: ~6%.
- $M = 10^6, \chi = 0.1$: ~1%.
- $M = 10^6, \chi = -0.1$: ~2%.

Larger body sizes ($M = 10^6$) have lower extinction risk due to reduced σ, and higher fat reserves further decrease the risk.

Figure 12 plots steady-state resource density (R_3^*) versus body mass (M) for the NSM, displaying two curves: $\chi = 0.1$ (high fat reserves, blue) and $\chi = -0.1$ (low fat reserves, red), across a logarithmic scale from 10^4 g to 1.748×10^7 g. It denotes the **competitive advantage of higher fat reserves**, with $\chi = 0.1$ showing lower R_3^* values (e.g., 0.237 vs. 0.366 at 10^4 g) compared to $\chi = -0.1$, supporting Cope's rule by illustrating that larger body sizes with greater fat reserves thrive with fewer resources, driving evolutionary size increase. The parameters used include fixed values such as $\mu = 0.1\,\mathrm{yr}^{-1}$ (mortality rate), $\xi = 1.0$ (recovery scaling), $\alpha = 1.0\,\mathrm{yr}^{-1}$ (resource growth rate), $\delta = 0.01$ and $\beta = 0.01$ (consumption rates), and allometric scaling coefficients $a_\lambda = 0.1$, $b_\sigma = 0.05$, and $c_\rho = 0.1$ for reproduction ($\lambda = a_\lambda M^{-3/4}$), starvation ($\sigma = b_\sigma M^{-1/4}(1+\chi)$), and recovery ($\rho = c_\rho M^{-1/4}(1+\chi)$) rates, respectively, with fat reserve adjustments via $\chi = 0.1$ and $\chi = -0.1$.

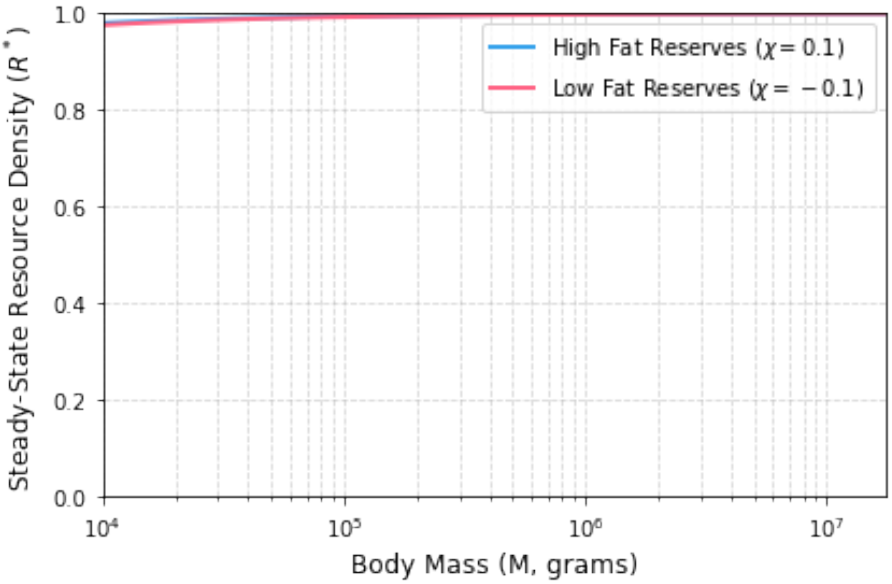

Figure 12. Resource density vs. body mass for different fat reserves.

The NSM supports Cope's rule by showing that larger body sizes and higher fat reserves reduce starvation rates and extinction risk, providing a selective advantage. Numerical analysis confirms

lower R_3^* for $\chi = 0.1$, supporting competitive superiority, and lower extinction probabilities for larger body sizes. The predicted M_{opt} and M_{max} align with fossil evidence. Limitations include the binary nutritional state assumption and herbivore focus, suggesting future extensions to continuous states or multi-species systems.

9. Conclusions

The NSM developed in this study offers a mechanistic understanding of how starvation and recovery dynamics shape the persistence of consumer-resource systems. By distinguishing between full and hungry consumer states, the model captures the energetic constraints and transitions that occur in resource-limited environments. Bifurcation analysis reveals a critical threshold at $\sigma = \lambda$, marking the transition between extinction and coexistence. When starvation outpaces reproduction ($\sigma > \lambda$), populations stabilize at sustainable densities with preserved resource levels, whereas higher reproduction ($\lambda > \sigma$) leads to instability and potential resource collapse. This framework identifies key thresholds—particularly the balance between reproduction and starvation rates—that enhance our understanding of population stability and extinction risk. The results demonstrate that tuning parameters, such as increasing fat reserves or adjusting energy allocation, can shift the system toward persistence, supporting evolutionary principles like Cope's rule. Furthermore, the ecological analogue of the basic reproduction number, $\mathcal{R}_e$, provides a clear threshold criterion distinguishing between population persistence and extinction within the starvation-recovery framework. By integrating theoretical analysis with numerical simulations, the NSM provides valuable insights into ecological resilience.

We can conclude this work by introducing some future directions.

Future research directions

- Study how changing λ and σ over time affects stability using simple periodic patterns.
- Explore random changes in resources with basic probability methods to see if extinction happens.
- Include a second consumer species and use simple competition rules to find coexistence conditions.
- Test a basic control method (like adding resources) to keep the system balanced and avoid extinction.

Use of Generative-AI tools declaration

The author declares that he has not used Artificial Intelligence (AI) tools in the creation of this article.

Funding

This work was supported by the Deanship of Scientific Research, Vice Presidency for Graduate Studies and Scientific Research, King Faisal University, Saudi Arabia [Grant No. 253958].

Conflict of interest

The author declares that he has no conflict of interest.

References

1. A. P. Allen, J. H. Brown, J. F. Gillooly, Global biodiversity, biochemical kinetics, and the energetic-equivalence rule, *Science*, **297** (2002), 1545–1548. https://doi.org/10.1126/science.1072380
2. S. Bentout, S. Kumar, S. Djilali, Hopf bifurcation analysis in an age-structured heroin model, *Eur. Phys. J. Plus*, **136** (2021), 260. https://doi.org/10.1140/epjp/s13360-021-01167-8
3. S. Bentout, S. Djilali, T. M. Touaoula, A. Zeb, A. Atangana, Bifurcation analysis for a double age dependence epidemic model with two delays, *Nonlinear Dyn.*, **108** (2022), 1821–1835. https://doi.org/10.1007/s11071-022-07234-8
4. S. Buitrago, R. Escalante, M. Villasana, A hybrid identification method for mathematical models for Zika virus, *Math. Methods Appl. Sci.*, **48** (2025), 14264–14275. https://doi.org/10.1002/mma.11176
5. N. Chitnis, J. M. Hyman, J. M. Cushing, Determining important parameters in the spread of malaria through the sensitivity analysis of a mathematical model, *Bull. Math. Biol.*, **70** (2008), 1272–1296. https://doi.org/10.1007/s11538-008-9299-0
6. P. Broadbridge, R. Cherniha, J. M. Goard, Exact nonclassical symmetry solutions of Lotka–Volterra type population systems, *Eur. J. Appl. Math.*, **34** (2023), 998–1016. https://doi.org/10.1017/S095679252200033X
7. A. Cintrón-Arias, C. Castillo-Chávez, L. Bettencourt, A. L. Lloyd, H. T. Banks, The estimation of the effective reproductive number from disease outbreak data, *Math. Biosci. Eng.*, **6** (2009), 261–282. https://doi.org/10.3934/mbe.2009.6.261
8. O. Diekmann, J. A. P. Heesterbeek, J. A. J. Metz, On the definition and computation of the basic reproduction ratio R_0 in models for infectious diseases in heterogeneous populations, *J. Math. Biol.*, **28** (1990), 365–382. https://doi.org/10.1007/BF00178324
9. É. Diz-Pita, M. Victoria Otero-Espinar, Predator–prey models: a review of some recent advances, *Mathematics*, **9** (2021), 1783. https://doi.org/10.3390/math9151783
10. A. A. Elsadany, A. M. Yousef, S. A. Ghazwani, A. S. Zaki, Bifurcation analysis of a discrete Basener–Ross population model: exploring multiple scenarios, *Computation*, **13** (2025), 11. https://doi.org/10.3390/computation13010011
11. B. J. Enquist, J. H. Brown, G. B. West, Allometric scaling of plant energetics and population density, *Nature*, **395** (1998), 163–165. https://doi.org/10.1038/25977
12. C. Hou, W. Zuo, M. E. Moses, W. H. Woodruff, J. H. Brown, G. B. West, Energy uptake and allocation during ontogeny, *Science*, **322** (2008), 736–739. https://doi.org/10.1126/science.1162302
13. C. P. Kempes, S. Dutkiewicz, M. J. Follows, Growth, metabolic partitioning, and the size of microorganisms, *Proc. Nat. Acad. Sci.*, **109** (2012), 495–500. https://doi.org/10.1073/pnas.1115585109

14. C. P. Kempes, C. Okegbe, Z. Mears-Clarke, L. E. Dietrich, Morphological optimization for access to dual oxidants in biofilms, *Proc. Nat. Acad. Sci.*, **111** (2014), 208–213. https://doi.org/10.1073/pnas.1315521110

15. A. Q. Khan, S. M. Qureshi, A. M. Alotaibi, Bifurcation analysis of a three species discrete-time predator-prey model, *Alex. Eng. J.*, **61** (2022), 7853–7875. https://doi.org/10.1016/j.aej.2021.12.068

16. M. O. Kulachi, A. Ahmad, E. Hincal, A. H. Ali, M. Farman, M. Taimoor, Control of conjunctivitis virus with and without treatment measures: a bifurcation analysis, *J. King Saud Univ.-Sci.*, **36** (2024), 103273. https://doi.org/10.1016/j.jksus.2024.103273

17. A. J. Lotka, Elements of physical biology, *Nature*, **116** (1925), 461. https://doi.org/10.1038/116461b0

18. N. A. Magnitskii, Universal bifurcation chaos theory and its new applications, *Mathematics*, **11** (2023), 2536. https://doi.org/10.3390/math11112536

19. S. Margenov, N. Popivanov, T. Hristov, V. Koleva, Computing the COVID-19 basic and effective reproduction numbers using actual data: SEIRS model with vaccination and hospitalization, *Mathematics*, **12** (2024), 3998. https://doi.org/10.3390/math12243998

20. A. Mezouaghi, S. Djilali, S. Bentout, K. Biroud, Bifurcation analysis of a diffusive predator–prey model with prey social behavior and predator harvesting, *Math. Methods Appl. Sci.*, **45** (2022), 718–731. https://doi.org/10.1002/mma.7807

21. M. Nadeem, O. A. Arqub, A. H. Ali, H. A. Neamah, Bifurcation, chaotic analysis and soliton solutions to the (3+1)-dimensional p-type model, *Alex. Eng. J.*, **107** (2024), 245–253. https://doi.org/10.1016/j.aej.2024.07.032

22. S. J. Pirt, The maintenance energy of bacteria in growing cultures, *Proc. R. Soc. London B: Biol. Sci.*, **163** (1965), 224–231. https://doi.org/10.1098/rspb.1965.0069

23. R. G. Romanescu, S. Hu, D. Nanton, M. Torabi, O. Tremblay-Savard, M. A. Haque, The effective reproductive number: modeling and prediction with application to the multi-wave COVID-19 pandemic, *Epidemics*, **44** (2023), 100708. https://doi.org/10.1016/j.epidem.2023.100708

24. M. S. Shabbir, Q. Din, M. De la Sen, J. F. Gómez-Aguilar, Exploring dynamics of plant–herbivore interactions: bifurcation analysis and chaos control with Holling type-II functional response, *J. Math. Biol.*, **88** (2024), 8. https://doi.org/10.1007/s00285-023-02020-5

25. N. H. Shah, J. Gupta, SEIR model and simulation for vector borne diseases, *Appl. Math.*, **4** (2013), 13–17. https://doi.org/10.4236/am.2013.48A003

26. M. B. Shapiro, F. Karim, G. Muscioni, A. S. Augustine, Adaptive susceptible-infectious-removed model for continuous estimation of the COVID-19 infection rate and reproduction number in the United States: modeling study, *J. Med. Int. Res.*, **23** (2021), e24389. https://doi.org/10.2196/24389

27. M. Swailem, U. C. Täuber, The Lotka–Volterra predator–prey model with periodically varying carrying capacity, *Phys. Rev. E*, **107** (2023), 064144. https://doi.org/10.1103/PhysRevE.107.064144

28. P. Van den Driessche, J. Watmough, Reproduction numbers and subthreshold endemic equilibria for compartmental models of disease transmission, *Math. Biosci.*, **180** (2002), 29–48. https://doi.org/10.1016/S0025-5564(02)00108-6

29. G. B. West, J. H. Brown, B. J. Enquist, A general model for ontogenetic growth, *Nature*, **413** (2001), 628–631. https://doi.org/10.1038/35098076

30. J. D. Yeakel, C. P. Kempes, S. Redner, Dynamics of starvation and recovery predict extinction risk and both Damuth's law and Cope's rule, *Nat. Commun.*, **9** (2018), 657. https://doi.org/10.1038/s41467-018-02822-y

31. G. M. Zelleke, M. I. Teboh-Ewungkem, G. A. Ngwa, Bifurcation analysis of a mathematical model for the activated complement-mediated response to bacterial infection in humans: the complement system as part of the innate immune system, *Adv. Cont. Discr. Mod.*, **2025** (2025), 90. https://doi.org/10.1186/s13662-025-03878-z

32. V. Volterra, Variazioni e fluttuazioni del numero d'individui in specie animali conviventi, *Memorie della Reale Accademia Nazionale dei Lincei*, Series VI, **2** (1926), 31–113.

AIMS Press